Acta Pharmaceutica Sinica B 2020;10(12):2362–2373

Chinese Pharmaceutical Association
Institute of Materia Medica, Chinese Academy of Medical Sciences

Acta Pharmaceutica Sinica B

www.elsevier.com/locate/apsb
www.sciencedirect.com

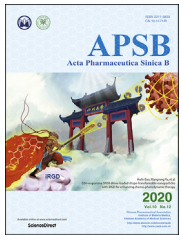

ORIGINAL ARTICLE

CORM-2-entrapped ultradeformable liposomes ameliorate acute skin inflammation in an ear edema model *via* effective CO delivery

Gwan-Yeong Lee[a,†], Alam Zeb[a,b,†], Eun-Hye Kim[a], Beomseon Suh[a], Young-Jun Shin[a], Donghyun Kim[a], Kyoung-Won Kim[a], Yeong-Hwan Choe[a], Ho-Ik Choi[a], Cheol-Ho Lee[a], Omer Salman Qureshi[c], In-Bo Han[d], Sun-Young Chang[e], Ok-Nam Bae[a,*], Jin-Ki Kim[a,*]

[a]*College of Pharmacy, Institute of Pharmaceutical Science and Technology, Hanyang University, Ansan 15588, Republic of Korea*
[b]*Riphah Institute of Pharmaceutical Sciences, Riphah International University, Islamabad 44000, Pakistan*
[c]*Department of Pharmacy, Forman Christian College, Lahore 54600, Pakistan*
[d]*Department of Neurosurgery, CHA Bundang Medical Center, School of Medicine, CHA University, Seongnam 13496, Republic of Korea*
[e]*College of Pharmacy, Ajou University, Suwon 16499, Republic of Korea*

Received 28 March 2020; received in revised form 16 May 2020; accepted 24 May 2020

KEY WORDS

Carbon monoxide;
CORM-2;
Anti-inflammatory effect;
Ultradeformable liposomes;
Skin inflammation;
Ear edema

Abstract The short release half-life of carbon monoxide (CO) is a major obstacle to the effective therapeutic use of carbon monoxide-releasing molecule-2 (CORM-2). The potential of CORM-2-entrapped ultradeformable liposomes (CORM-2-UDLs) to enhance the release half-life of CO and alleviate skin inflammation was investigated in the present study. CORM-2-UDLs were prepared by using soy phosphatidylcholine to form lipid bilayers and Tween 80 as an edge activator. The deformability of CORM-2-UDLs was measured and compared with that of conventional liposomes by passing formulations through a filter device at a constant pressure. The release profile of CO from CORM-2-UDLs was evaluated by myoglobin assay. *In vitro* and *in vivo* anti-inflammatory effects of CORM-2-UDLs were assessed in lipopolysaccharide-stimulated macrophages and TPA-induced ear edema model, respectively. The

*Corresponding authors. Tel.: +82 31 4005805; fax: +82 31 4005958 (Ok-Nam Bae); Tel.: +82 31 4005808; fax: +82 31 4005958 (Jin-Ki Kim).
E-mail addresses: onbae@hanyang.ac.kr (Ok-Nam Bae), jinkikim@hanyang.ac.kr (Jin-Ki Kim).
†The authors made equal contributions to this work.

Peer review under responsibility of Chinese Pharmaceutical Association and Institute of Materia Medica, Chinese Academy of Medical Sciences.

https://doi.org/10.1016/j.apsb.2020.05.010

deformability of the optimized CORM-2-UDLs was 2.3 times higher than conventional liposomes. CORM-2-UDLs significantly prolonged the release half-life of CO from 30 s in a CORM-2 solution to 21.6 min. CORM-2-UDLs demonstrated *in vitro* anti-inflammatory activity by decreasing nitrite production and pro-inflammatory cytokine levels. Furthermore, CORM-2-UDLs successfully ameliorated skin inflammation by reducing ear edema, pathological scores, neutrophil accumulation, and inflammatory cytokines expression. The results demonstrate that CORM-2-UDLs could be used as promising therapeutics against acute skin inflammation.

1. Introduction

In the past few decades, low molecular weight gaseous molecules, including nitric oxide (NO), carbon monoxide (CO) and hydrogen sulfide (H_2S), have been well recognized as gasotransmitters in human and have attracted attention because of their novel therapeutic potential[1,2]. The beneficial biological effects of CO remained unexplored for a long time owing to its reputation for toxicity, arising from its 250-fold higher binding affinity toward hemoglobin (Hb) compared with oxygen, which causes tissue hypoxia by substantially reducing the oxygen-carrying capacity of Hb[3,4]. However, endogenously produced CO has been shown to exhibit a variety of valuable biological functions, such as anti-inflammatory, anti-apoptotic, anti-proliferative, anti-oxidant, vasoactive and cytoprotective activities[5,6]. The endogenous production of CO in human bodies results from the catabolism of heme by heme oxygenase (HO) enzymes. The heme degradation pathway involves the activity of the inducible isoform HO-1 and the constitutive isoform HO-2 to produce equimolar quantities of CO, biliverdin and free iron[7]. The HO-1 pathway is activated in response to stressful insults, such as ischemia, hypoxia, inflammation, apoptotic signals and redox imbalance, so it generates physiological concentrations of CO to act as a signaling molecule for the regulation of intracellular, neural and vascular functions[8].

The recognition of the biological functions of endogenous CO has led scientists to investigate the therapeutic benefits of exogenously administered CO. The potent anti-inflammatory activity of inhaled CO is well established in animal models of inflammation, ischemia, lung and vascular injuries, sepsis and graft rejection[9−12]. A major hurdle in the effective clinical utility of direct CO inhalation is the need for strict dose control and specialized settings because overdosing on CO can be lethal[5,13]. These problems have prompted the design of innovative carbon monoxide-releasing molecules (CORMs) to serve as CO donors and safely deliver gaseous CO. CORMs are transition metal carbonyl complexes, capable of releasing controlled amounts of CO when exposed to a suitable biological environment. Some noteworthy CORMs that have already been developed are CORM-1 [$Mn_2(CO)_{10}$ and $Fe(CO)_5$], CORM-2 [$Ru(CO)_3Cl_2]_2$, CORM-3 [$Ru(CO)_3$Cl-glycinate] and CORM-A_1 [$Na_2(H_3BCO_2)$][14]. CORMs use a unique strategy to release their CO payload in the body and have been reported to exhibit the therapeutic potential of CO in a variety of animal models[15,16]. The overwhelming majority of previous studies have focused on the commercially available CORM-2, proving its anti-inflammatory, antimicrobial, anti-allodynic, anti-nociceptive and anti-hyperalgesic effects[17−19]. However, the clinical utility of CORM-2 remains a challenge because its CO release half-life is less than a minute[8]. Nanoparticle-mediated delivery of CORM-2 is one promising approach to solve the problem of its short CO release profile.

The therapeutic effectiveness of CORM-2 has been improved in several studies by loading it in nanoparticles that then release the CO in a controlled manner. The encapsulation of CORM-2 in styrene-maleic acid copolymer micelles resulted in better tissue protection, compared with free CORM-2, against inflammatory bowel disease in a murine colitis model[20]. In a subsequent study by our group[21], sustained CO release from CORM-2-loaded solid lipid nanoparticles enhanced its *in vivo* anti-inflammatory effects in a carrageenan-induced rat paw edema model. Most recently, we found that loading CORM-2 in solid lipid nanoparticles enhanced its anti-allodynic and anti-hyperalgesic effects in a chronic constriction injury model[22]. Our group, for the first time, is exploring the potential of CORM-2-loaded nanocarriers in a skin inflammation model. The next generation of liposomes, often described as elastic, deformable, or ultradeformable liposomes (UDLs) or Tansfersomes™, holds great promise for improving the skin permeation of therapeutic agents[23,24]. UDLs are a spherical, nanosized drug delivery system composed of bilayers of phospholipid molecules and an edge activator[25]. The presence of edge activator in the phospholipid bilayers enables UDLs to penetrate deep into the skin by using a hydration gradient across the epidermis[26]. In contrast to UDLs, conventional liposomes contain cholesterol instead of an edge activator in their bilayers, which limits their ability to permeate the skin. Therefore, UDLs might not only be a promising way to improve the skin permeation of CORM-2 to ameliorate skin inflammation, but they might also function to enhance the CO release half-life.

In this study, we investigated the anti-inflammatory potential of CORM-2-entrapped ultradeformable liposomes (CORM-2-UDLs) in a tetradecanoylphorbol acetate (TPA)-induced skin inflammation model. CORM-2-UDLs, which used soy phosphatidylcholine (SPC) to form the bilayer and Tween 80 (TW80) as an edge activator, were prepared and optimized using a lipid film hydration and extrusion technique. They were characterized for particle size, polydispersity index (PDI), surface charge, entrapment efficiency, deformability and morphology. The release of CO from CORM-2-UDLs was assessed using myoglobin assay, and *in vitro* and *in vivo* anti-inflammatory effects were evaluated using lipopolysaccharide-stimulated macrophages and ear edema model, respectively.

2. Materials and methods

2.1. Materials

The SPC was kindly gifted by Lipoid GmbH (Ludwigshafen, Germany). CORM-2, TW80, sodium dithionite, myoglobin, mineral oil, Griess reagent, TPA, 3-(4,5-dimethylthiazol-2-yl)-2,5-diphenyltetrazolium bromide (MTT) and lipopolysaccharide (LPS) were purchased from Sigma−Aldrich (St. Louis, MO, USA), and fetal bovine serum (FBS) and Dulbecco's modified Eagle's medium (DMEM) were purchased from Gibco BRL (Grand Island, NY, USA). All other chemicals were of analytical grade and were used without any further purification.

2.2. Preparation of CORM-2-UDLs

CORM-2-UDLs, which used SPC to form the lipid bilayer and TW80 as the edge activator, were prepared by a slightly modified thin lipid film hydration and extrusion technique[27]. Concisely, CORM-2, SPC, and TW80 were dissolved in chloroform that was then evaporated at a reduced pressure using a rotary evaporator (Rotavapor R-3; Büchi Labortechnik AG, Flawil, Switzerland). Further drying of the resultant thin lipid film was accomplished by purging it with a stream of nitrogen gas for 30 min. The completely dried lipid film was hydrated with a 5% dextrose solution maintained at a temperature (40 °C) above the phase transition of SPC. The obtained liposomal dispersion was sonicated for 30 min in a bath type sonicator operated at 40 °C and then extruded 6-times through a 100 nm polycarbonate membrane using a Mini-Extruder (Avanti Polar Lipids, Inc., Alabaster, AL, USA). The resultant CORM-2-UDLs were further purified by removing free CORM-2 through an ultrafiltration centrifugation process at 14,000×*g* for 15 min and stored in a refrigerator (4 °C) until further analysis. The composition of CORM-2-UDLs is presented in Table 1.

2.3. Particle size, PDI, surface charge and entrapment efficiency of CORM-2-UDLs

Suitably diluted samples of CORM-2-UDLs were analyzed with a light-scattering instrument (Zetasizer Nano ZS; Malvern Instruments, Malvern, UK) to determine the mean particle size, PDI and surface charge in terms of zeta potential. The particle size measurement and PDI are based on photon correlation spectroscopy, and the zeta potential evaluation is based on the principle of electrophoretic light scattering.

The amount of CORM-2 entrapped in CORM-2-UDLs was determined by measuring the amount of ruthenium (Ru) in the sample with inductively coupled plasma atomic emission spectrophotometry (Spectro, Kleve, Germany) at a detection wavelength of 240.3 nm[22]. The entrapment efficiency (%) of CORM-2-UDLs was then calculated using Eq. (1) as follow.

$$\text{Entrapment efficiency (\%)} = \frac{\text{Amount of Ru in CORM-2-UDLs}}{\text{Total amount of Ru in CORM-2 added}} \times 100 \quad (1)$$

The optimized CORM-2-UDLs formulation was evaluated for storage stability at 4 and 25 °C for 28 days. For this purpose, CORM-2-UDLs were stored in dry and sealed glass vials flushed with a stream of nitrogen gas. Samples were subsequently monitored for changes in particle size, PDI, zeta potential and entrapment efficiency at Days 1, 3, 7, 14, 21 and 28.

2.4. Deformability index of CORM-2-UDLs

The deformability index of UDLs measures their ability to penetrate pores much smaller than their own diameter. The deformability of CORM-2-UDLs was measured by extruding the sample through a 50 nm polycarbonate membrane in a stainless steel pressure extruder (Lipix Extruder; Northern Lipids Inc., Burnaby, BC, Canada) at a constant pressure of 0.1 MPa[28]. The deformability index (D) was then calculated by measuring the volume of CORM-2-UDLs extruded in 5 min (J) and their particle size after extrusion (r_v) through a permeability barrier having pore diameter (r_p) of 50 nm, using the following equation Eq. (2).

$$D = J \times \left(\frac{r_v}{r_p}\right)^2 \quad (2)$$

2.5. Transmission electron microscopy

The morphological features of the optimized CORM-2-UDLs were visualized using a field-emission transmission electron microscope (FE-TEM, JEM-2100F; JEOL, Tokyo, Japan). The sample was prepared for TEM analysis by adding a drop of CORM-2-UDLs formulation onto a carbon-coated 400 mesh copper grid, and allowing surface adsorption. The excess CORM-2-UDLs were removed from the grid, and then we added a drop of 1% phosphotungstic acid solution for negative staining. The negatively stained sample was properly dried at room temperature and analyzed with TEM at an accelerating voltage of 200 kV[29].

Table 1 Composition and physicochemical properties of CORM-2-UDLs.

Formulation	Composition (*w*/*w*)			Physicochemical properties			
	SPC	TW80	CORM-2	Particle size (nm)	PDI	Zeta potential (mV)	Entrapment efficiency (%)
CORM-2-UDLs-T1	9	1	1	106.3 ± 1.6	0.070 ± 0.025	43.7 ± 4.9	35.5 ± 0.9
CORM-2-UDLs-T2	8	2	1	100.9 ± 1.5	0.087 ± 0.025	42.7 ± 4.5	31.5 ± 2.0
CORM-2-UDLs-T3	7	3	1	98.6 ± 3.1	0.116 ± 0.005	40.9 ± 4.8	27.1 ± 2.3
CORM-2-UDLs-T4	6	4	1	95.3 ± 1.2	0.141 ± 0.031	38.0 ± 6.8	23.9 ± 2.0

SPC: soy phosphatidylcholine, TW80: Tween 80, UDLs: ultradeformable liposomes, CORM-2: carbon monoxide-releasing molecule-2, PDI: polydispersity index. Data are expressed as the mean ± SD (n = 3).

2.6. *In vitro CO release from CORM-2-UDLs*

In vitro release profile of CO from CORM-2-UDLs was evaluated with a myoglobin assay[21,30]. Precisely, myoglobin (Mb) solution was prepared by dissolving lyophilized equine heart Mb in phosphate-buffered saline (0.01 mol/L, pH 7.4). Sodium dithionite (0.1%, *w/v*) was added as a reducing agent to 1 mL of Mb solution to accomplish the conversion of Mb into deoxyMb. CORM-2-UDLs or CORM-2 solution in ethanol (equivalent to 20 μmol/L CORM-2) was then directly mixed with 1 mL of deoxyMb solution in a quartz cuvette. The resultant reaction mixture was covered with 500 μL of light mineral oil to prevent the escape of the released CO and oxygenation of the deoxyMb to Mb. The amount of carbonmonoxy myoglobin (MbCO) produced from the deoxyMb as a result of CO release from CORM-2-UDLs or CORM-2 solution was quantified by measuring the optical density at 510 and 540 nm using a UV−Visible spectrophotometer (Ultrospec 7000, Biochrom Ltd., Cambridge, UK). The produced MbCO was quantified at regular intervals until the release of CO reached a plateau.

2.7. *In vitro cell viability and anti-inflammatory studies*

2.7.1. *Cell culture*

A RAW 264.7 cell line of murine macrophages was purchased from the American Type Culture Collection (Manassas, VA, USA). The macrophage cells were cultured in DMEM containing 10% heat-inactivated FBS, 100 μg/mL of streptomycin, and 100 units/mL of penicillin. The cells were cultured at 37 °C in humidified air containing 5% CO_2. Experiments were conducted when the cell cultures reached ~80% confluence.

2.7.2. *MTT assay*

The effects of CORM-2-UDLs and CORM-2 solution on *in vitro* cell viability were measured by the MTT assay to confirm that the formulations did not produce cytotoxicity in living cells. Briefly, RAW 264.7 cells were seeded in 96-well plates at a density of 1×10^4 cells/well and incubated at 37 °C for 24 h. The cells were treated and incubated with two different concentrations of CORM-2-UDLs and CORM-2 solution (equivalent to 10 and 20 μmol/L of CORM-2) for 24 h. Each well was then treated with MTT reagent (0.5 mg/mL) followed by incubation for an additional 2 h at 37 °C. After the supernatant was carefully removed, formazan crystals in each well were dissolved by the addition of 100 μL of DMSO. Formazan concentration was determined by measuring the absorbance at 570 nm using a multimode spectrophotometer (Enspire, PerkinElmer, Waltham, MA, USA), and the cell viability (%) was calculated by comparing the absorbance with that of untreated control cells[31].

2.7.3. *Nitric oxide assay*

In vitro anti-inflammatory effects of CORM-2-UDLs were evaluated in LPS-stimulated RAW 264.7 cells using a NO assay[31]. The amount of a pro-inflammatory mediator, NO, that the cells produced was measured as an indicator of inflammation. For this purpose, RAW 264.7 cells were seeded in 24-well plates at a density of 1×10^5 cells/well and incubated at 37 °C for 24 h. The cells were subsequently challenged with LPS (200 ng/mL) for 24 h in the absence or presence of CORM-2-UDLs and CORM-2 solution (at a dose equivalent to 10 and 20 μmol/L of CORM-2). The supernatant from each well was collected and centrifuged to remove cell debris, which was followed by the addition of Griess reagent and subsequent incubation for an additional 20 min at room temperature. The ability of CORM-2-UDLs to inhibit LPS-stimulated NO production was measured by quantifying the nitrite concentration (stable end product of NO) at 540 nm using a multimode spectrophotometer (Enspire, PerkinElmer, Waltham, MA, USA). A standard calibration curve of sodium nitrite was constructed to calculate the nitrite concentration.

2.7.4. *Measurement of pro-inflammatory cytokines level*

In vitro anti-inflammatory effects of CORM-2-UDLs were further evaluated by measuring the production of pro-inflammatory cytokines in LPS-stimulated RAW 264.7 cells. The cytokines were quantified in terms of released protein and mRNA expression levels using an enzyme-linked immunosorbent assay (ELISA) and quantitative real-time polymerase chain reaction (qRT-PCR), respectively. RAW 264.7 cells were stimulated with LPS (200 ng/mL) for 24 h in the absence or presence of CORM-2-UDLs and CORM-2 solution (at a dose equivalent to 20 μmol/L of CORM-2), as described for NO assay. The released levels of IL-6, IL-1β, and TNF-α in the cells supernatant were determined by using their respective mouse DuoSet ELISA kit (R&D systems, Minneapolis, MN, USA), according to the manufacturer's instructions.

The levels of mRNA expression for IL-6, IL-1β, and TNF-α were determined by qRT-PCR. For this purpose, RAW 264.7 cells were stimulated with LPS (200 ng/mL) for 24 h in the absence or presence of CORM-2-UDLs and CORM-2 solution (at a dose equivalent to 20 μmol/L of CORM-2), followed by total RNA isolation from the cells using TRIzol reagent (Life Technologies, Carlsbad, CA, USA) according to the manufacturer's protocol[32]. Purified RNA (500 ng) was reverse transcribed to synthetize cDNA by using ReverTra Ace® RT kit (Toyobo, Osaka, Japan) in MyCycler™ Thermal Cycler (Bio-Rad Laboratories Inc., Hercules, CA, USA). Quantitative PCR was performed using iQTM SYBR Green supermix (Bio-Rad) on a CFX96TM Real-Time PCR Detection System (Bio-Rad), under the conditions of 95 °C for 10 min, followed by 45 cycles at 98 °C for 10 s, 60 °C for 30 s, and 72 °C for 1 min, and elongation at 72 °C for 5 min. The primers were obtained from Genotech (Daejeon, Republic of Korea), and the sequences for mouse primers were as follows: for *Gapdh*, sense 5′-TGAACGGGAAGCTCACTGG-3′ and anti-sense 5′-TCCACCACCCTGTTGCTGTA-3′; for IL-1β, sense 5′-CAACCAACAAGTGATATTCTCCATG-3′ and anti-sense 5′-GATCCACACTCTCCAGCTGCA-3′; for IL-6, sense 5′-AACGATGATGCACTTGCAGA-3′ and anti-sense 5′-GAGCATTGGAAATTGGGGTA-3′;for TNF-α, sense 5′-ATGAGCACAGAAAGCATGATC-3′ and anti-sense 5′-TACAGGCTTGTCACTCGAATT-3′. Gene expressions were calculated using the comparative CT method ($2^{-\Delta\Delta Ct}$), and normalized to the GAPDH control.

2.8. *In vivo anti-inflammatory activity of CORM-2-UDLs*

2.8.1. *TPA-induced ear edema model*

In vivo anti-inflammatory activity of CORM-2-UDLs was investigated in a TPA-induced mouse model of ear edema[33]. Male ICR mice (6 weeks old) were purchased from the Koatech Laboratory Animal Company (Pyeongtaek, Gyeonggi, Republic of Korea). All animal experiments were approved by the Institutional Animal Care and Use Committee of Hanyang University, and all procedures were conducted according to the guidelines of the National Institutes of Health. Concisely,

CORM-2-UDLs (equivalent to 0.2 mg of CORM-2), CORM-2 solution (0.2 mg of CORM-2), indomethacin (0.2 mg), or vehicle (20 μL of 5% dextrose) was applied on the inner and outer skin surface of the right ear, followed by the application of TPA (2 μg/ear) on the same ear after 1 h. The left ear of each animal was used as the control.

2.8.2. Ear thickness and weight measurement

The extent of edema in the TPA-induced mouse model was assessed by measuring the thickness and weight of the right and left ears of each animal. At the designated time intervals of 0, 1, 2, 3, 4, 5, and 6 h following TPA application, the thickness of each ear was measured with a digital caliper. Six hours after TPA application, the mice were sacrificed, and a plug 6 mm in diameter was removed from both ears with a biopsy punch (Kai Industries, Tokyo, Japan) and weighed. The difference in the thickness and weight of the right and left ears in each mouse was used to determine the treatment effects of CORM-2-UDLs. The collected ear plugs were further processed and evaluated for histopathological changes and the expression of different inflammatory mediators.

2.8.3. Histopathological analysis

The tissue samples collected from the right ears of the mice were fixed in 4% neutral buffered paraformaldehyde solution for histopathological analysis. The preserved tissue samples were embedded in paraffin, and cross sections were prepared followed by hematoxylin and eosin (H&E) staining. Histological changes and cellular infiltration were examined by analyzing the stained sections under a light microscope. The slides were observed by a histologist blinded to the experimental conditions for the number of neutrophils per scope, and pathological scores were assigned for ear edema (0−5), epidermal hyperproliferation (0−5), and leucocyte infiltration (0−5).

2.8.4. Estimation of cytokine mRNA levels in ear tissues

In vivo levels of mRNA expression of *Il-6, Il-1β, and Tnf-α* in ear tissues were estimated by qRT-PCR. The samples collected from the right ears were frozen, homogenized, and total RNA from tissue homogenates was isolated with the TRIzol reagent using the manufacturer's protocol. Complementary DNA was created by reverse transcribing purified total RNA (500 ng) with a ReverTra Ace® qPCR RT Kit (Toyobo, Osaka, Japan) in a MyCycler™ Thermal Cycler (Bio-Rad). qRT-PCR was performed with iQTM SYBR Green Supermix on a CFX96TM Real-Time PCR Detection System (Bio-Rad). The detailed conditions for qRT-PCR and the primer sequences were same with those in the *in vitro* studies as described above.

2.9. Statistical analysis

All the experiments in this study were repeated at least three times, and the data are presented as the mean ± standard deviation (SD) or standard error of mean (SEM). Statistical analysis of data was carried out by applying the Student's *t*-test or one-way ANOVA with *post hoc* Duncan's or Mann−Whitney U testing using SPSS software (SPSS Inc., Chicago, IL, USA). A value of $P < 0.05$ was regarded as a statistically significant difference.

3. Results

3.1. Preparation and characterization of CORM-2-UDLs

CORM-2-UDLs were prepared and optimized with different ratios of SPC (lipid bilayer former) and TW80 (deformability inducing edge activator) using the popular thin lipid film hydration method. The cumulative amount of SPC and TW80 was kept constant at 10 mg/mL, and a fixed amount of CORM-2 (1 mg/mL) was added to all formulations. The ratios of SPC to TW80 were varied as 9:1, 8:2, 7:3, and 6:4 (*w/w*) to optimize the composition of CORM-2-UDLs for particle size, PDI, entrapment efficiency, and deformability. The results of physicochemical characterization of CORM-2-UDLs are described in Table 1. All CORM-2-UDL formulations produced an average particle size of around 100 nm with PDI values of <0.200, demonstrating a narrow size distribution of liposomal vesicles. The distribution pattern of CORM-2-UDLs showed a unimodal curve (Fig. 1A), which indicates a homogenous size distribution in the vesicle dispersion. The surfaces of CORM-2-UDLs were positively charged, as demonstrated by zeta potential values of around 40 mV. The maximum entrapment efficiency was 35.5% (CORM-2-UDLs-T1), which was subsequently reduced to 23.9% when the amount of edge activator in the lipid bilayers was increased from 1 to 4 mg/mL (CORM-2-UDLs-T4). On the other hand, increasing the TW80 concentration had a negligible effect on the particle size and PDI values of CORM-2-UDLs. These results indicate that CORM-2-UDLs possess the favorable physicochemical properties required of nano-particulate drug delivery systems.

One of the key and unique attributes of UDLs is their ability to deform their shape for enhanced skin penetration. The shape transformation ability of CORM-2-UDLs was measured in terms of a deformability index, and the results are depicted in Fig. 1B. CORM-2-UDLs had significantly higher deformability indices than conventional liposomes (CORM-2-CLs). In addition, the deformability of CORM-2-UDLs was greatly influenced by the concentration of the edge activator in the lipid bilayers. The deformability indices increased in the order of CORM-2-CLs (19.5 ± 2.8)<CORM-2-UDLs-T4 (28.3 ± 2.6)<CORM-2-UDLs-T3 (36.0 ± 3.6)<CORM-2-UDLs-T1 (37.7 ± 0.6)<CORM-2-UDLs-T2 (44.1 ± 3.2), representing about 1.46, 1.84, 1.93, and 2.26 times higher deformability by CORM-2-UDLs compared with CORM-2-CLs. These results indicate that the pliability of the lipid bilayers decreased when the TW80 concentration increased beyond 2 mg/mL, *i.e.*, with SPC:TW80 ratios of 7:3 and 6:4 (-T3 and -T4 formulations). Based on their highest deformability index and reasonable entrapment efficiency, CORM-2-UDLs-T2 (SPC:TW80 = 8:2, *w/w*) were chosen as the optimized formulation for all further experiments.

The optimized formulation, CORM-2-UDLs-T2, was then subjected to TEM analysis to visualize its morphology, and the resultant micrograph is shown in Fig. 1C. The TEM image revealed a spherical shape with vesicular morphology, with a distinct lipid bilayer surrounding an inner aqueous core. The unilamellar and uniform shape of CORM-2-UDLs accompanied nanometric dimensions (~100 nm), thereby validating the results of the photon correlation spectroscopy size analysis. The optimized CORM-2-UDLs-T2 formulation was also evaluated for storage stability at refrigerator and room temperatures (4 and 25 °C) for a period of 28 days (Table 2). CORM-2-UDLs maintained its physicochemical properties at 4 °C as shown by the absence of any marked changes in particle size, PDI, zeta potential

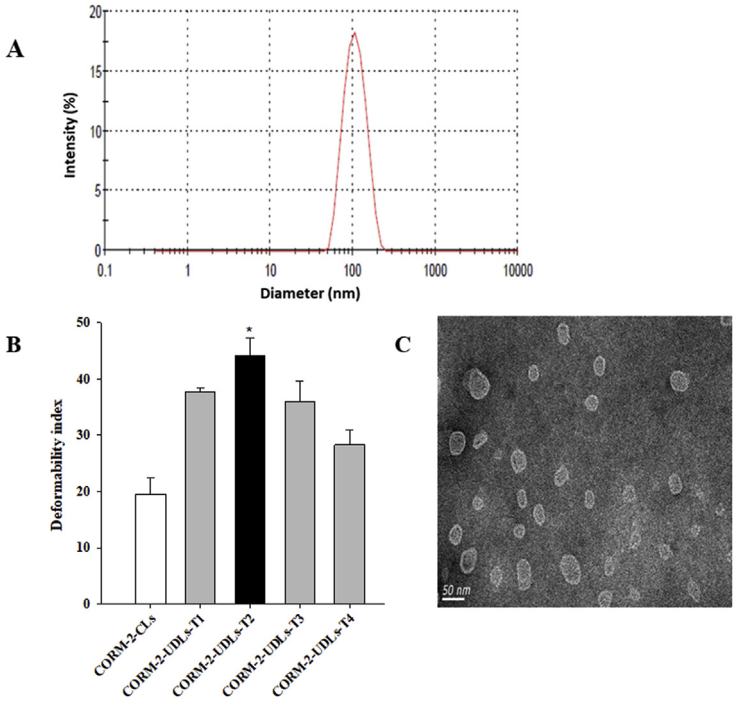

Figure 1 Physicochemical characterization of CORM-2-UDLs. (A) Particle size distribution, (B) deformability indices and (C) TEM image of CORM-2-UDLs. The deformability indices are expressed as the mean ± SD ($n = 3$). *$P < 0.05$ *vs.* CORM-2-CLs, CORM-2-UDLs-T1, CORM-2-UDLs-T3, and CORM-2-UDLs-T4.

Table 2 Storage stability of CORM-2-UDLs at 4 and 25 °C for 28 days.

Day	Particle size (nm)		PDI		Zeta potential (mV)		Entrapment efficiency (%)	
	4 °C	25 °C	4 °C	25 °C	4 °C	25 °C	4 °C	25 °C
0	100.9 ± 1.5	100.9 ± 1.5	0.087 ± 0.025	0.087 ± 0.025	42.7 ± 4.5	42.7 ± 4.5	31.5 ± 2.0	31.5 ± 2.0
1	99.8 ± 2.6	99.2 ± 2.9	0.059 ± 0.016	0.085 ± 0.016	45.2 ± 6.8	41.7 ± 2.6	31.4 ± 2.0	30.9 ± 2.6
3	98.1 ± 2.3	96.8 ± 3.6	0.087 ± 0.003	0.083 ± 0.028	42.2 ± 1.0	41.8 ± 1.6	30.5 ± 1.8	29.9 ± 1.9
7	100.3 ± 0.8	97.6 ± 3.5	0.085 ± 0.019	0.071 ± 0.007	46.3 ± 3.7	37.4 ± 4.6	30.1 ± 2.8	27.4 ± 2.0
14	99.0 ± 5.9	95.9 ± 2.4	0.077 ± 0.013	0.067 ± 0.010	45.2 ± 4.4	22.6 ± 1.7	29.0 ± 2.0	24.6 ± 3.3
21	97.9 ± 3.2	89.5 ± 3.2	0.077 ± 0.029	0.067 ± 0.002	45.1 ± 3.2	7.7 ± 1.3	28.0 ± 1.1	23.2 ± 3.9
28	99.2 ± 1.7	89.5 ± 4.3	0.067 ± 0.020	0.079 ± 0.021	40.2 ± 6.0	3.5 ± 1.0	27.2 ± 2.5	15.5 ± 4.1

Data are expressed as the mean ± SD ($n = 3$).

and entrapment efficiency after 28 days. In contrary, substantial decrease in zeta potential (42.7 *vs.* 3.5 mV) and entrapment efficiency (31.5% *vs.* 15.5%) was observed at 25 °C. These findings indicate a superior storage stability of CORM-2-UDLs at low temperature compared with room temperature and therefore advocate the need for storage at refrigerator conditions.

3.2. *CO release profile of CORM-2-UDLs*

The release of CO from CORM-2-UDLs and its subsequent binding to deoxyMb in the myoglobin assay was quantitatively determined by monitoring spectrophotometric changes upon the formation of MbCO. The time-course release profile of CO from CORM-2-UDLs over a period of 3 h is illustrated in Fig. 2A. CORM-2-UDLs exhibited controlled CO release, in contrast to the instant release seen with CORM-2 solution. In the initial 30 min, ~90% of the CO was released from CORM-2 solution, whereas CORM-2-UDLs took 75 min to release the same amount of CO. Furthermore, CORM-2-UDLs maintained a slow and continuous release pattern of CO for 2 h. A detailed depiction and comparison of CO release from CORM-2-UDLs and CORM-2 solution in the initial 20 min is shown in Fig. 2B. It is evident that CORM-2 solution released 74% and 87% of its CO in 3 and 20 min, respectively, whereas CORM-2-UDLs released only 1.8% and 48% of their CO during the same times. It is noteworthy that CORM-2-UDLs extended the release half-life of CO by up to 43 times compared with CORM-2 solution (21.6 min *vs.* 30 s).

3.3. *Effects of CORM-2-UDLs on cell viability and LPS-stimulated inflammatory responses*

The non-cytotoxicity of CORM-2-UDLs was confirmed by measuring the viability of macrophage cells using the MTT assay (Fig. 3A). Treatment of cells with CORM-2-UDLs or CORM-2 solution at 10 and 20 μmol/L concentrations did not produce any cytotoxic effects, as evidenced by cell viability of >95% of

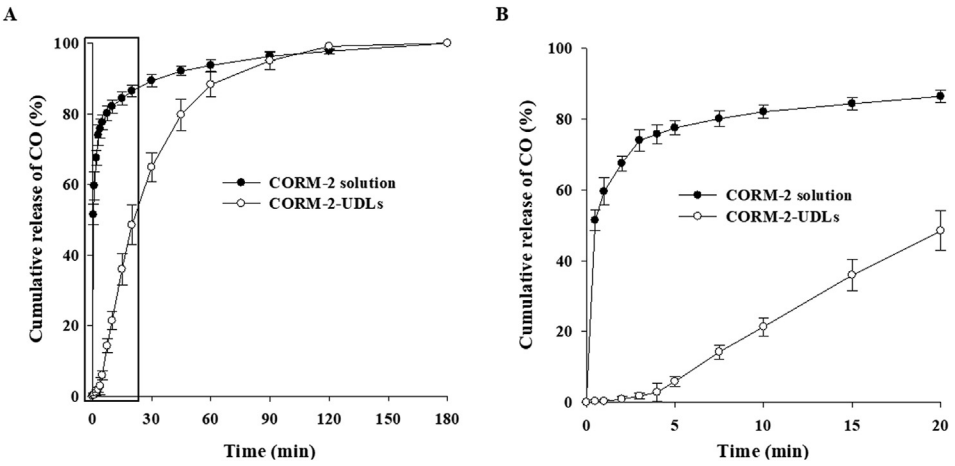

Figure 2 *In vitro* CO release profiles of CORM-2-UDLs and CORM-2 solution determined by myoglobin assay. (A) CO release for 180 min and (B) CO release for initial 20 min. Data are expressed as the mean ± SD ($n = 3$).

that found in the untreated control cells. These results suggest that CORM-2 and all the ingredients used to formulate CORM-2-UDLs are nontoxic and safe for *in vivo* use.

To investigate the anti-inflammatory effects of CORM-2-UDLs, the suppression of LPS-stimulated increase in the inflammatory mediators, such as nitric oxide (NO) and cytokines in RAW 264.7 macrophage cells was measured. The amount of NO was quantified in terms of nitrite concentration, and the results are presented in Fig. 3B. The inhibitory effects of CORM-2-UDLs on nitrite production were evaluated at concentrations of 10 and 20 μmol/L and were compared with the effects of CORM-2 solution using untreated LPS-stimulated cells as a control. At 10 μmol/L, CORM-2-UDLs significantly reduced ($P < 0.01$) the nitrite concentration to 36.8%, much lower than that from cells treated with CORM-2 solution (75.5%). Similarly, a remarkable difference in the suppression of nitrite production was seen between CORM-2-UDLs (18.4%) and CORM-2 solution (66.4%) at the 20 μmol/L dose. These results suggest that CORM-2-UDLs have potent *in vitro* anti-inflammatory effects. A dose of 20 μmol/L of CORM-2 was selected for further *in vitro* anti-inflammatory studies, since it demonstrated a better inhibitory effects on the nitrite production compared to 10 μmol/L dose in NO assay.

The pro-inflammatory cytokines are known to play important roles in the amplification of inflammation through transcriptional regulation. While the levels of released cytokines in media increased after LPS stimulation, the increase was significantly suppressed in macrophages treated with CORM-2-UDLs (Fig. 4A). The levels of IL-6 (37.2%), IL-1β (9.0%) and TNF-α (55.2%) were significantly decreased by CORM-2-UDLs in comparison with CORM-2 solutions (93.5%, 63.9% and 86.9% for each cytokine), suggesting that CORM-2-UDLs effectively blocked the amplification of inflammation mediated by different cytokines. To further confirm the inhibitory effects of CORM-2-UDLs on cytokine production, the mRNA levels of cytokines were measured by qRT-PCR following 24 h treatment with LPS in the presence or absence of CORM-2. Both the IL-6 mRNA (34.5%) and TNF-α mRNA (32.0%) were significantly reduced by CORM-2-UDLs (Fig. 4B), consistent to the level of released cytokines. The mRNA expression levels of IL-1β (163.8%) in LPS-stimulated macrophages at 24 h were not statistically different between CORM-2-UDLs and CORM-2 solution groups.

3.4. Alleviation of skin inflammation by CORM-2-UDLs

3.4.1. Effects of CORM-2-UDLs on ear edema

In vivo anti-inflammatory effects of CORM-2-UDLs were assessed in mice using the TPA-induced ear edema model. Topical application of TPA results in the induction of acute skin inflammation accompanied by severe ear edema[34]. The severity of ear edema was monitored by measuring the difference in thickness between the right (treated) and left (untreated) ears (Fig. 5A). The ear thickness started to rise following TPA application, with a substantial increase to 0.43 ± 0.02 mm in the TPA group after 6 h, compared with the vehicle control group, which had an almost constant thickness throughout the monitoring period. As shown in Fig. 5A, differences in the edema levels among treatment groups were noticeable as early as 2 h after TPA application and continued to increase for 6 h. With the indomethacin (positive control) and CORM-2 solution treatments, the ear thickness recorded after 6 h was 0.32 ± 0.02 and 0.33 ± 0.04 mm, respectively, both significantly lower than the TPA-treated group ($P < 0.05$). On the contrary, prominently less ear edema was observed in CORM-2-UDL group, whose ear thickness was only 0.08 ± 0.01 mm, which was close to that of the vehicle group. CORM-2 solution displayed results comparable to those of the positive control (indomethacin), with edema levels higher than those in CORM-2-UDL group, demonstrating that CORM-2-UDLs more effectively attenuated skin inflammation. In addition to ear thickness, the weight of the ear plugs was also reduced significantly by CORM-2-UDLs (2.18 ± 0.64 mg) compared with the TPA only (14.82 ± 0.45 mg), indomethacin (12.22 ± 0.75 mg), and CORM-2 solution (13.36 ± 1.35 mg) treated groups (Fig. 5B). These results demonstrate the significant *in vivo* anti-inflammatory activity of CORM-2-UDLs.

3.4.2. Macroscopic observation and microscopic evaluation of ear tissues after H&E staining

TPA-induced real-time changes were visually observed, and histopathological attributes and the accumulation of inflammatory cells in ear tissue were microscopically detected after H&E staining (Fig. 6). Real-time photographs indicate that the severity of TPA-induced ear edema was successfully reduced by CORM-2-UDL treatment, as evidenced by a decrease in swelling and erythema. Similarly, the infiltration and accumulation of

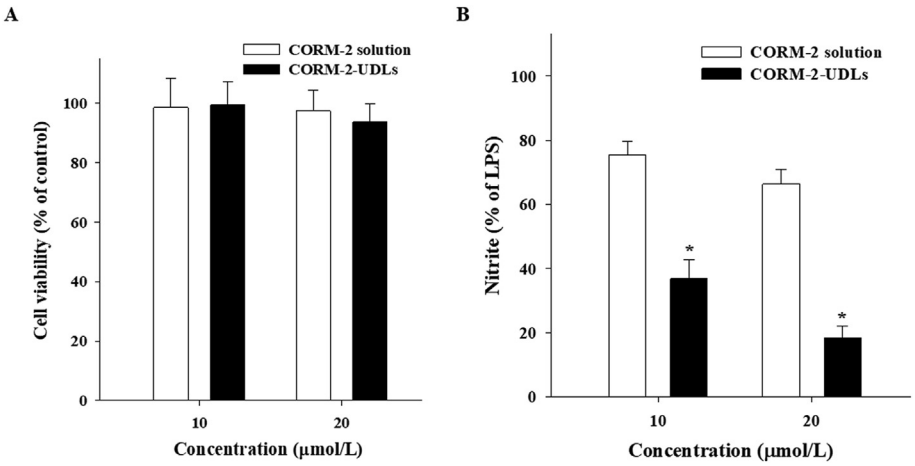

Figure 3 (A) Cell viability and (B) *in vitro* anti-inflammatory effects of CORM-2-UDLs and CORM-2 solution in RAW 264.7 cells. To assess *in vitro* anti-inflammatory effects, cells were stimulated with lipopolysaccharide and the nitrite concentration was determined. Data are expressed as the mean ± SD ($n = 5$). *$P < 0.01$ *vs.* CORM-2 solution.

inflammatory cells decreased remarkably at the inflamed sites, and normal tissue architecture was preserved by CORM-2-UDLs, as observed in the microscopic images (Fig. 6A). In contrast, indomethacin and CORM-2 solution had less prominent effects on cellular infiltration and tissue architecture than CORM-2-UDLs. The neutrophil count (Fig. 6B) increased after TPA application (157 cells/scope) and was more substantially reduced by CORM-2-UDLs (10 cells/scope) than by the indomethacin (69 cells/scope) or CORM-2 solution (110 cells/scope). Furthermore, pathological indicators of skin inflammation, ear edema, epidermal hyperproliferation, and leukocyte infiltration, were scored by a histologist blinded to the experimental conditions and tabulated in Table 3. CORM-2-UDL samples exhibited 3.1, 2.6, and 2.5 times lower histological scores for ear edema (1.13) compared with the TPA (3.53), indomethacin (2.93), and CORM-2 solution (2.87) groups, respectively. Likewise, epidermal hyperproliferation and leukocyte infiltration scores were also significantly lower in CORM-2-UDL group than in the animals assigned to the TPA, indomethacin, and CORM-2 solution groups. Taking the results of the histopathological evaluation together, CORM-2-UDLs efficiently ameliorated all the representative parameters of skin inflammation in the TPA-induced ear edema model.

3.4.3. *Evaluation of cytokine expression*

Tissue samples from the right ear of each animal were evaluated for the expression of potent pro-inflammatory cytokines, *Il-6, Il-1β, and Tnf-α,* in the skin (Fig. 7). Topical application of TPA alone significantly increased the expression of those mediators in the mouse ears compared with the vehicle group. The mRNA expression level of *Il-6* was significantly lower in CORM-2-UDL group (1.75-fold) than in the TPA (217-fold), indomethacin (168-fold), and CORM-2 solution (289-fold) groups (Fig. 7A). Similarly, CORM-2-UDL-treated mice showed 16.6, 5.6, and 7.7 times lower expression of *Il-1β* (1.91) than mice treated with TPA only (31.77), indomethacin (10.69), or CORM-2 solution (14.78), respectively (Fig. 7B). The effects of indomethacin and CORM-2 solution on the mRNA expression levels of *Il-1β* were comparable to each other, and both were substantially less than in TPA only group. Furthermore, *Tnf-α* expression levels were also markedly reduced by CORM-2-UDLs (Fig. 7C). The suppression of pro-inflammatory cytokines, accompanied by the alleviation of ear edema and improved histopathological scores, suggest the therapeutic potential of topically applied CORM-2-UDLs against skin inflammation.

4. Discussion

Despite the well-recognized potent anti-inflammatory effects of CO, its therapeutic applications are restricted by safety and dose control requirements[11]. CORM-2 is an attractive alternative to gaseous CO, however, it releases CO very quickly and thereby reduces its usefulness as a CO donor in animal models. In this study, we developed CORM-2-UDLs to both prolong the release half-life of CO and improve skin permeation to produce anti-inflammatory effects against skin inflammation. CORM-2-UDLs were prepared from SPC and TW80, which are both physiologically biocompatible, pharmaceutically acceptable, and widely studied ingredients[23,35,36]. The concentrations of SPC and TW80 were varied to study the influence of composition and obtain CORM-2-UDLs with optimal physiochemical properties. We observed that the particle size of CORM-2-UDLs decreased slightly (106.3−95.3 nm) with a higher ratio of TW80 (9:1 *vs.* 6:4, SPC:TW80), possibly because the insertion of TW80 in the lipid bilayer membranes produced an increased curvature and reduced the diameter of the UDLs[37]. Increasing the amount of TW80 in the vesicles bilayers reduced the entrapment efficiency of CORM-2-UDLs from 35.5% to 23.9%. CORM-2 is a lipophilic moiety that is concurrently accommodated in the SPC matrix with TW80. A higher TW80 content not only diminished the overall volume of the lipid bilayers by decreasing the particle size but also reduced their capacity to accommodate CORM-2, which reduced the entrapment efficiency in CORM-2-UDLs. In addition, pore formation in the lipid bilayers with a higher edge activator concentration was previously associated with lower drug entrapment efficiency in UDLs[38].

Edge activator-imparted deformability is an important feature because CORM-2-UDLs were formulated for topical delivery. In comparison to conventional liposomes, CORM-2-UDLs demonstrated higher deformability indices at each concentration of TW80. It has been reported that edge activators cause shape transformations in UDLs exposed to mechanical stress or space detention. That stress-dependent adaptability could be attributed

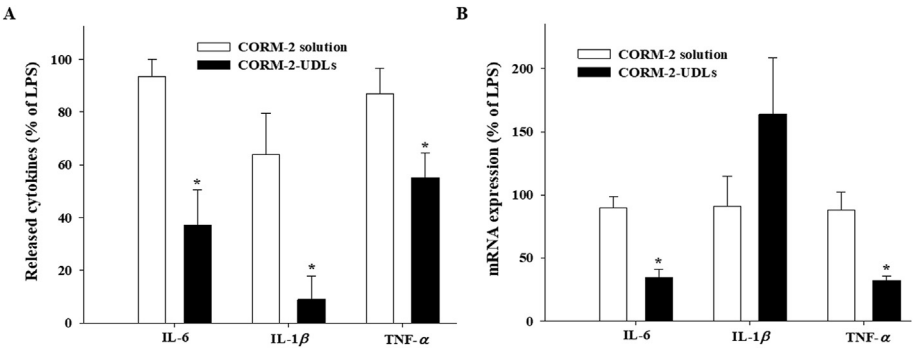

Figure 4 The inhibitory effects of CORM-2-UDLs on the pro-inflammatory cytokines in LPS-stimulated RAW 264.7 cells. (A) The level of IL-6, IL-1β and TNF-α determined by ELISA and (B) the expression of mRNA for IL-6, IL-1β and TNF-α detected by quantitative real-time PCR. Data are expressed as the mean ± SEM ($n = 3$). *$P < 0.05$ *vs.* CORM-2 solution group.

to the repositioning of TW80 and SPC molecules, enabling CORM-2-UDLs to penetrate pores with dimensions many times smaller than their own[39,40]. It is worth mentioning that edge activators are mostly single chain surfactants with a high curvature radius and mobility, so they produce lipid vesicles with a low elastic modulus and thereby bring about shape adaptability at low energy[41]. The deformability of the bilayer membranes decreased at high TW80 concentration (3 and 4 mg/mL), possibly because of the coexistence of mixed micelles with less flexible structures[38]. On the other hand, the complete absence of an edge activator in the bilayer membranes of CORM-2-CLs rendered them too rigid to penetrate small pores[29]. CORM-2-UDLs-T2 formulation (SPC:TW80 of 8:2), which had the highest deformability, was chosen as the optimized formulation and used in all further experiments. The storage conditions play a vital role in the stability of liposomal formulations since lipid vesicles have a natural propensity to fuse and disintegrate upon storage and thereby bring about drug leakage and changes in their particle size, PDI and surface charge[27,42]. The enhanced stability of CORM-2-UDLs at low temperature could be ascribed to the fact that higher temperature escalates the kinetic energy and collision of the lipid vesicles. In addition, lipid bilayer degradation and defective membrane packing are also prominent at higher temperature due to gel-to-liquid transitions resulting in compromised storage stability[43].

Our findings indicate that CORM-2-UDLs substantially slowed the release and enhanced the half-life of CO. It is a sequential process consisting of slower CORM-2 release from the lipid bilayer matrix of CORM-2-UDLs followed by instant liberation of the CO from CORM-2 upon ligand substitution triggered by sodium dithionite[44]. The rate-controlling step in the overall release process is the diffusion and degradation of the liposomal bilayer membrane, which releases the entrapped CORM-2. In contrast, in CORM-2 solution, CORM-2 was readily available for ligand substitution with sodium dithionite, which resulted in immediate CO release. On the basis of their extended CO release kinetics, we expected CORM-2-UDLs to display superior *in vitro* and *in vivo* anti-inflammatory responses in cells and animal models.

Experimental evidence indicates that the therapeutic effectiveness of CO depends strongly on the concentration, mode, and duration of its application, apart from other pathophysiological parameters[6]. This dependence necessitates strict and precise control of CO release from CORM-2 for its safe and efficient use against inflammatory conditions. Slower CO release from CORM-2-UDLs, which produced longer exposure for the macrophages, resulted in improved *in vitro* anti-inflammatory activity in the NO assay and cytokines analysis. The smaller reduction in nitrite and cytokine concentrations seen with CORM-2 solution could be ascribed to its instant release of CO, which causes a rapid loss of anti-inflammatory action. It is noteworthy that CO liberated from CORM-2 was shown to suppress nitrite formation and the inflammatory response by inhibiting NO synthase in an LPS-challenged cell culture system[45]. Furthermore, it has also been reported that CO treatment modulates the production and polarization of macrophages towards M2 phenotype, thereby inhibiting the release of pro-inflammatory cytokines and increasing the secretion of anti-inflammatory cytokines in RAW 264.7 cells[46,47]. Those findings provide a reasonable explanation for the effects of CORM-2-UDLs and CORM-2 solution observed in our study. *In vivo* alleviation of acute skin inflammation following topical application of CORM-2-UDLs was confirmed in murine TPA-induced ear edema, a well-recognized and widely used model of localized skin inflammation characterized by increased epidermal proliferation and thickness, the infiltration of inflammatory cells, and elevated levels of pro-inflammatory cytokines in dermal tissues[34,48]. Compared with CORM-2 solution and indomethacin control, the enhanced *in vivo* anti-inflammatory activity seen with CORM-2-UDLs was consistent with the results from *in vitro* NO and cytokine assay. CORM-2-UDLs successfully suppressed the inflammatory parameters of skin edema, histological changes, the accumulation of neutrophils, and cytokine expression (IL-6, IL-1β and TNF-α). While we observed consistent anti-inflammatory effects of CORM-2-UDLs throughout *in vitro* and *in vivo* results, there was a discrepancy between the mRNA level and protein level of IL-1β in the *in vitro* cell system (Fig. 4A and B). We could not observe a statistically significant inhibition of IL-1β mRNA level at 24 h after LPS stimulation. On the other hand, the released level of IL-1β, which may play more actual role in inflammatory amplification than mRNA itself, was significantly reduced by CORM-2-UDLs. This might be due to the different time window of mRNA expression and the cytokine release during dynamic inflammatory processes. Since the mRNA expression of IL-1β is maximally induced at ~6 h after LPS stimulation and gradually decreased according to the time[49], it would be worthy to examine IL-1β mRNA level at earlier time point to clarify the inhibitory effect of CORM-2-UDLs on IL-1β at the transcriptional level. The level of mRNA expression of *Il-1β* as well as *Il-6* and *Tnf-α* was significantly reduced by CORM-2-UDLs in mouse ear samples at 4 h after inflammation induction, supporting the regulation of cytokines by CORM-2-UDLs in transcription level.

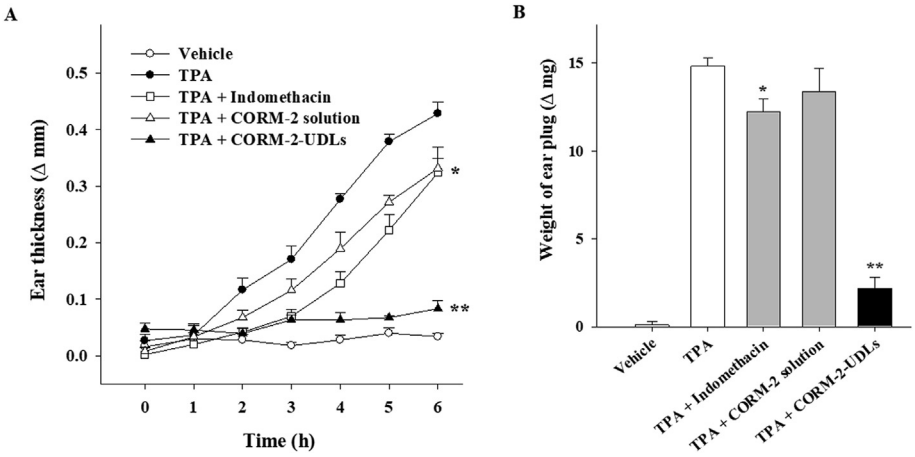

Figure 5 Suppression of TPA-induced skin inflammation after treatment with CORM-2-UDLs. (A) The severity of edema evaluated by ear thickness and (B) the weight of ear plugs. Data are expressed as the mean ± SEM ($n = 5$). *$P < 0.05$ *vs.* TPA group and **$P < 0.01$ *vs.* CORM-2 solution group.

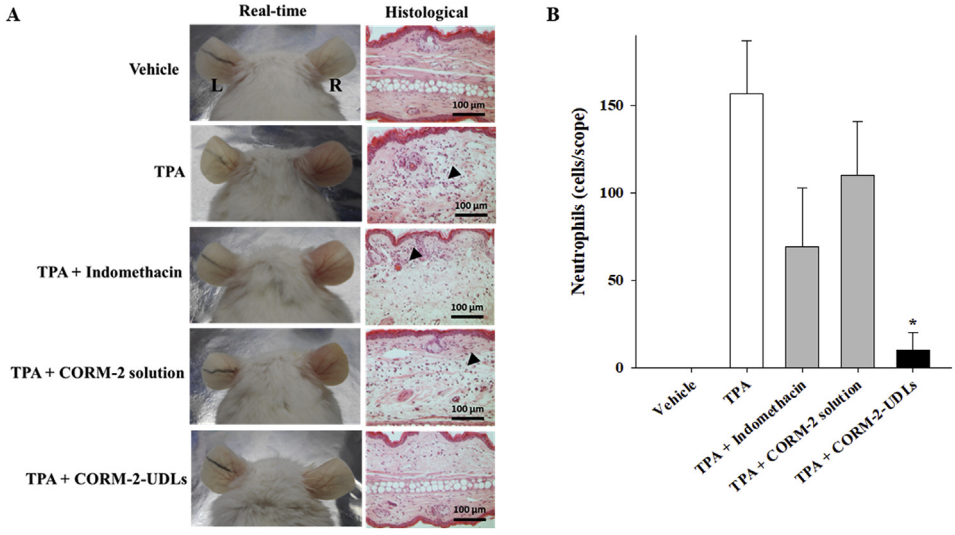

Figure 6 Macroscopic observation and histopathological evaluation of ear tissues after H&E staining. (A) Real-time images and histological micrographs and (B) neutrophil counts per scope of ear tissues. Data are expressed as the mean ± SEM ($n = 5$). *$P < 0.01$ *vs.* TPA group, TPA + indomethacin group, and TPA + CORM-2 solution group.

Table 3 Effects of CORM-2-UDLs on pathological parameters in TPA-induced ear edema model.

Group	Ear edema	Epidermal hyperproliferation	Leucocyte infiltration
Vehicle	0.00 ± 0.00	0.00 ± 0.00	0.00 ± 0.00
TPA	3.53 ± 0.38	2.47 ± 0.69	3.27 ± 0.43
TPA + indomethacin	2.93 ± 0.43	1.47 ± 0.30	2.60 ± 0.15
TPA + CORM-2 solution	2.87 ± 0.56	1.93 ± 0.72	2.53 ± 0.65
TPA + CORM-2-UDLs	1.13 ± 0.77$^{\#}$	0.93 ± 0.72*	0.73 ± 0.55$^{\#}$

Data are expressed as the mean ± SD ($n = 5$). *$P < 0.01$ *vs.* TPA and $^{\#}P < 0.01$ *vs.* TPA, TPA + indomethacin and TPA + CORM-2 solution groups.

Percutaneous permeability of CORM-2-UDLs into the inflamed tissues is needed to exert *in vivo* anti-inflammatory effects. The permeation of CORM-2-UDLs into the deeper skin strata is facilitated by the edge activator-induced ultradeformability of the vesicles, which promotes dermal accumulation[50]. In addition to shape deformation, the interaction and subsequent destabilization of intercellular lipids by the UDLs is a mechanism contributing to enhanced drug deposition in the skin layers[51,52]. It has also been reported that the permeation of UDLs is followed by continuous drug release based on their

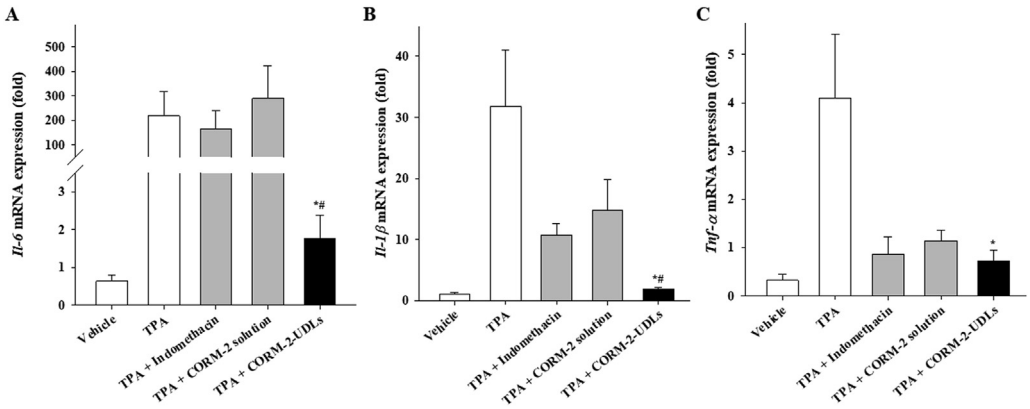

Figure 7 Effects of CORM-2-UDLs on the expression of mRNA for inflammatory cytokines. (A) *Il-6*, (B) *Il-1β* and (C) *Tnf-α*. Data are expressed as the mean ± SEM ($n = 5$). $^{*}P < 0.05$ *vs.* TPA group and $^{\#}P < 0.01$ *vs.* CORM-2 solution group.

solubility in the stratum corneum lipids[53]. Because it is a lipophilic moiety, CORM-2 can partition and diffuse well into the skin lipids. To dissociate CO in the biological milieu, CORM-2 requires ligand substitution preferably with thiol-containing compounds[54]. Glutathione, cysteine, and proteins with free cysteine residues are probably the main ligands that trigger CO release from CORM-2 in the skin layers[30,55]. Taken together, our results indicate that our CORM-2-UDLs successfully delivered CO into inflamed skin and produced anti-inflammatory effects.

5. Conclusions

Our data demonstrate that (i) CORM-2-UDLs extended the release half-life of CO *via* slower and constant release of CORM-2; (ii) CORM-2-UDLs enhanced the skin permeation and dermal accumulation of CORM-2; and (iii) CORM-2-UDLs showed superior anti-inflammatory effects in LPS-stimulated RAW 264.7 macrophages and the murine TPA-induced ear edema model compared with CORM-2 solution. Consequently, topical application of CORM-2-UDLs could be a potential therapeutic approach to suppressing skin inflammation in biological models.

Acknowledgments

This work was supported by the Basic Science Research Program of the National Research Foundation of Korea (NRF) funded by the Ministry of Science and ICT (NRF-2017R1A2B4006458).

Author contributions

Gwan-Yeong Lee and Alam Zeb conceptualized the study, designed and conducted the experiments, performed data analysis and wrote the manuscript. Beomseon Suh, Young-Jun Shin, Donghyun Kim, Kyoung-Won Kim and Yeong-Hwan Choe developed *in vitro* and *in vivo* experimental models. Eun-Hye Kim, Ho-Ik Choi and Cheol-Ho Lee performed additional experiments in the revision. Omer Salman Qureshi, In-Bo Han and Sun-Young Chang assisted in data analysis, *in vivo* experiments and writing, review and editing of the manuscript. Ok-Nam Bae and Jin-Ki Kim supervised the project, managed funding, interpreted the data and reviewed the manuscript. All of the authors have read and approved the final manuscript.

Conflicts of interest

The authors have no conflicts of interest to declare related to this work.

References

1. Ryter SW, Choi AM. Carbon monoxide: present and future indications for a medical gas. *Korean J Intern Med* 2013;**28**:123–40.
2. Zheng Y, Ji X, Ji K, Wang B. Hydrogen sulfide prodrugs—a review. *Acta Pharm Sin B* 2015;**5**:367–77.
3. Rose JJ, Wang L, Xu Q, McTiernan CF, Shiva S, Tejero J, et al. Carbon monoxide poisoning: pathogenesis, management, and future directions of therapy. *Am J Respir Crit Care Med* 2017;**195**:596–606.
4. Piantadosi CA. Biological chemistry of carbon monoxide. *Antioxidants Redox Signal* 2002;**4**:259–70.
5. Motterlini R, Otterbein LE. The therapeutic potential of carbon monoxide. *Nat Rev Drug Discov* 2010;**9**:728–43.
6. Bauer I, Pannen BH. Bench-to-bedside review: carbon monoxide-from mitochondrial poisoning to therapeutic use. *Crit Care* 2009;**13**:220.
7. Abraham NG, Kappas A. Pharmacological and clinical aspects of heme oxygenase. *Pharmacol Rev* 2008;**60**:79–127.
8. Motterlini R, Mann BE, Foresti R. Therapeutic applications of carbon monoxide-releasing molecules. *Expet Opin Invest Drugs* 2005;**14**:1305–18.
9. Otterbein LE, Mantell LL, Choi AM. Carbon monoxide provides protection against hyperoxic lung injury. *Am J Physiol* 1999;**276**:L688–94.
10. Fujita T, Toda K, Karimova A, Yan SF, Naka Y, Yet SF, et al. Paradoxical rescue from ischemic lung injury by inhaled carbon monoxide driven by derepression of fibrinolysis. *Nat Med* 2001;**7**:598–604.
11. Foresti R, Bani-Hani MG, Motterlini R. Use of carbon monoxide as a therapeutic agent: promises and challenges. *Intensive Care Med* 2008;**34**:649–58.
12. Otterbein LE, Zuckerbraun BS, Haga M, Liu F, Song R, Usheva A, et al. Carbon monoxide suppresses arteriosclerotic lesions associated with chronic graft rejection and with balloon injury. *Nat Med* 2003;**9**:183–90.
13. Romão CC, Blättler WA, Seixas JD, Bernardes GJL. Developing drug molecules for therapy with carbon monoxide. *Chem Soc Rev* 2012;**41**:3571–83.
14. García-Gallego S, Bernardes GJ. Carbon-monoxide-releasing molecules for the delivery of therapeutic CO *in vivo*. *Angew Chem* 2014;**53**:9712–21.
15. Ismailova A, Kuter D, Bohle DS, Butler IS. An overview of the potential therapeutic applications of CO-releasing molecules. *Bioinorgan Chem Appl* 2018;**2018**:8547364.

16. Kourti M, Jiang WG, Cai J. Aspects of carbon monoxide in form of CO-releasing molecules used in cancer treatment: more light on the way. *Oxid Med Cell Longev* 2017;**2017**:9326454.
17. Wei Y, Chen P, de Bruyn M, Zhang W, Bremer E, Helfrich W. Carbon monoxide-releasing molecule-2 (CORM-2) attenuates acute hepatic ischemia reperfusion injury in rats. *BMC Gastroenterol* 2010;**10**:42.
18. Takagi T, Naito Y, Uchiyama K, Suzuki T, Hirata I, Mizushima K, et al. Carbon monoxide liberated from carbon monoxide-releasing molecule exerts an anti-inflammatory effect on dextran sulfate sodium-induced colitis in mice. *Dig Dis Sci* 2011;**56**:1663−71.
19. Nobre LS, Seixas JD, Romao CC, Saraiva LM. Antimicrobial action of carbon monoxide-releasing compounds. *Antimicrob Agents Chemother* 2007;**51**:4303−7.
20. Yin H, Fang J, Liao L, Nakamura H, Maeda H. Styrene-maleic acid copolymer-encapsulated CORM2, a water-soluble carbon monoxide (CO) donor with a constant CO-releasing property, exhibits therapeutic potential for inflammatory bowel disease. *J Control Release* 2014;**187**:14−21.
21. Qureshi OS, Zeb A, Akram M, Kim M-S, Kang JH, Kim HS, et al. Enhanced acute anti-inflammatory effects of CORM-2-loaded nanoparticles *via* sustained carbon monoxide delivery. *Eur J Pharm Biopharm* 2016;**108**:187−95.
22. Joshi HP, Kim SB, Kim S, Kumar H, Jo MJ, Choi H, et al. Nanocarrier-mediated delivery of CORM-2 enhances anti-allodynic and anti-hyperalgesic effects of CORM-2. *Mol Neurobiol* 2019;**56**:5539−54.
23. Zeb A, Arif ST, Malik M, Shah FA, Din FU, Qureshi OS, et al. Potential of nanoparticulate carriers for improved drug delivery *via* skin. *J Pharm Investig* 2019;**49**:485−517.
24. Maniyar MG, Kokare CR. Formulation and evaluation of spray dried liposomes of lopinavir for topical application. *J Pharm Investig* 2019;**49**:259−70.
25. Elsayed MMA, Abdallah OY, Naggar VF, Khalafallah NM. Lipid vesicles for skin delivery of drugs: reviewing three decades of research. *Int J Pharm* 2007;**332**:1−16.
26. Cevc G, Blume G. Lipid vesicles penetrate into intact skin owing to the transdermal osmotic gradients and hydration force. *Biochim Biophys Acta* 1992;**1104**:226−32.
27. Zeb A, Qureshi OS, Kim HS, Cha JH, Kim HS, Kim JK. Improved skin permeation of methotrexate *via* nanosized ultradeformable liposomes. *Int J Nanomed* 2016;**11**:3813.
28. Gupta PN, Mishra V, Rawat A, Dubey P, Mahor S, Jain S, et al. Non-invasive vaccine delivery in transfersomes, niosomes and liposomes: a comparative study. *Int J Pharm* 2005;**293**:73−82.
29. Zeb A, Cha JH, Noh AR, Qureshi OS, Kim KW, Choe YH, et al. Neuroprotective effects of carnosine-loaded elastic liposomes in cerebral ischemia rat model. *J Pharm Investig* 2020;**50**:373−81.
30. Hasegawa U, van der Vlies AJ, Simeoni E, Wandrey C, Hubbell JA. Carbon monoxide-releasing micelles for immunotherapy. *J Am Chem Soc* 2010;**132**:18273−80.
31. Akram M, Syed Ahmed S, Kim KA, Lee Jong S, Chang SY, Kim Chul Y, et al. Heme oxygenase 1-mediated novel anti-inflammatory activities of *Salvia plebeia* and its active components. *J Ethnopharmacol* 2015;**174**:322−30.
32. Akram M, Kim KA, Kim ES, Shin YJ, Noh D, Kim E, et al. Selective inhibition of JAK2/STAT1 signaling and iNOS expression mediates the anti-inflammatory effects of coniferyl aldehyde. *Chem Biol Interact* 2016;**256**:102−10.
33. Akram M, Shin I, Kim KA, Noh D, Baek SH, Chang SY, et al. A newly synthesized macakurzin *C*-derivative attenuates acute and chronic skin inflammation: the Nrf 2/heme oxygenase signaling as a potential target. *Toxicol Appl Pharmacol* 2016;**307**:62−71.
34. Bralley EE, Greenspan P, Hargrove JL, Wicker L, Hartle DK. Topical anti-inflammatory activity of *Polygonum cuspidatum* extract in the TPA model of mouse ear inflammation. *J Inflamm* 2008;**5**:1.
35. Chen J, Lu WL, Gu W, Lu SS, Chen ZP, Cai BC. Skin permeation behavior of elastic liposomes: role of formulation ingredients. *Expet Opin Drug Deliv* 2013;**10**:845−56.
36. Hussain A, Singh S, Sharma D, Webster TJ, Shafaat K, Faruk A. Elastic liposomes as novel carriers: recent advances in drug delivery. *Int J Nanomed* 2017;**12**:5087−108.
37. Duangjit S, Pamornpathomkul B, Opanasopit P, Rojanarata T, Obata Y, Takayama K, et al. Role of the charge, carbon chain length, and content of surfactant on the skin penetration of meloxicam-loaded liposomes. *Int J Nanomed* 2014;**9**:2005.
38. El Zaafarany GM, Awad GA, Holayel SM, Mortada ND. Role of edge activators and surface charge in developing ultradeformable vesicles with enhanced skin delivery. *Int J Pharm* 2010;**397**:164−72.
39. Cevc G, Blume G. Biological activity and characteristics of triamcinolone-acetonide formulated with the self-regulating drug carriers, Transfersomes®. *Biochim Biophys Acta* 2003;**1614**:156−64.
40. Perez AP, Altube MJ, Schilrreff P, Apezteguia G, Celes FS, Zacchino S, et al. Topical amphotericin B in ultradeformable liposomes: formulation, skin penetration study, antifungal and antileishmanial activity *in vitro*. *Colloids Surf B Biointerfaces* 2016;**139**:190−8.
41. Cevc G. Rational design of new product candidates: the next generation of highly deformable bilayer vesicles for noninvasive, targeted therapy. *J Control Release* 2012;**160**:135−46.
42. Dubey V, Mishra D, Dutta T, Nahar M, Saraf DK, Jain NK. Dermal and transdermal delivery of an anti-psoriatic agent *via* ethanolic liposomes. *J Control Release* 2007;**123**:148−54.
43. Dubey V, Mishra D, Jain NK. Melatonin loaded ethanolic liposomes: physicochemical characterization and enhanced transdermal delivery. *Eur J Pharm Biopharm* 2007;**67**:398−405.
44. McLean S, Mann BE, Poole RK. Sulfite species enhance carbon monoxide release from CO-releasing molecules: implications for the deoxymyoglobin assay of activity. *Anal Biochem* 2012;**427**:36−40.
45. Sawle P, Foresti R, Mann BE, Johnson TR, Green CJ, Motterlini R. Carbon monoxide-releasing molecules (CO-RMs) attenuate the inflammatory response elicited by lipopolysaccharide in RAW264.7 murine macrophages. *Br J Pharmacol* 2005;**145**:800−10.
46. Otterbein LE, Bach FH, Alam J, Soares M, Lu HT, Wysk M, et al. Carbon monoxide has anti-inflammatory effects involving the mitogen-activated protein kinase pathway. *Nat Med* 2000;**6**:422.
47. Taguchi K, Nagao S, Maeda H, Yanagisawa H, Sakai H, Yamasaki K, et al. Biomimetic carbon monoxide delivery based on hemoglobin vesicles ameliorates acute pancreatitis in mice *via* the regulation of macrophage and neutrophil activity. *Drug Deliv* 2018;**25**:1266−74.
48. Castro J, Rivera D, Franco LA. Topical anti-inflammatory activity in TPA-induced mouse ear edema model and *in vitro* antibacterial properties of Cordia alba flowers. *J Pharm Investig* 2019;**49**:331−6.
49. Yu WG, He H, Yao JY, Zhu YX, Lu YH. Dimethyl cardamonin exhibits anti-inflammatory effects *via* interfering with the PI3K-PDK1-PKCalpha signaling pathway. *Biomol Ther* 2015;**23**:549−56.
50. Cosco D, Paolino D, Maiuolo J, Di Marzio L, Carafa M, Ventura CA, et al. Ultradeformable liposomes as multidrug carrier of resveratrol and 5-fluorouracil for their topical delivery. *Int J Pharm* 2015;**489**:1−10.
51. Elsayed MMA, Abdallah OY, Naggar VF, Khalafallah NM. Deformable liposomes and ethosomes: mechanism of enhanced skin delivery. *Int J Pharm* 2006;**322**:60−6.
52. Benson HA. Transfersomes for transdermal drug delivery. *Expet Opin Drug Deliv* 2006;**3**:727−37.
53. Honeywell-Nguyen PL, Bouwstra JA. The *in vitro* transport of pergolide from surfactant-based elastic vesicles through human skin: a suggested mechanism of action. *J Control Release* 2003;**86**:145−56.
54. Kautz AC, Kunz PC, Janiak C. CO-releasing molecule (CORM) conjugate systems. *Dalton Trans* 2016;**45**:18045−63.
55. Markina M, Stozhko N, Krylov V, Vidrevich M, Brainina K. Nanoparticle-based paper sensor for thiols evaluation in human skin. *Talanta* 2017;**165**:563−9.